Available online at www.sciencedirect.com
ScienceDirect
Journal of Membrane Science 318 (2008) 45–55
journal of MEMBRANE SCIENCE
www.elsevier.com/locate/memsci

Hydrogen separation from reforming gas using organic templating silica/alumina composite membrane

Jong-Ho Moon [a], Ji-Han Bae [a], Youn-Sang Bae [a], Jong-Tae Chung [a,b], Chang-Ha Lee [a,*]

[a] *Department of Chemical Engineering, Yonsei University, Seoul, Republic of Korea*
[b] *Hydrogen & Fuel Cell R & D division, Korea Gas Corporation, Incheon, Republic of Korea*

Received 10 October 2007; received in revised form 30 January 2008; accepted 3 February 2008
Available online 12 February 2008

Abstract

The separation characteristics and dynamics of hydrogen mixture produced from natural gas reformer were studied on methyltriethoxysilane (MTES) templating silica membrane. The permeation and separation of CO pure gas, H_2/CO (50/50, vol.%) binary mixture and $H_2/CH_4/CO/CO_2$ (69/3/2/26, vol.%) quaternary mixture were investigated both experimentally and theoretically. Since the permeance of pure CO on the MTES membrane was very low (CO ≈ 4.79–6.46×10^{-11} mol m^{-2} s^{-1} Pa^{-1}), comparatively high hydrogen selectivity could be obtained from the H_2/CO mixture (separation factor = 93–110). This implies that CO, which should be eliminated prior to use in fuel cells, can be separated from hydrogen mixtures using MTES membranes. The permeance of the H_2 quaternary mixture on the MTES membrane was 2.07–3.37×10^{-9} mol m^{-2} s^{-1} Pa^{-1} and the separation factor of $H_2/(CO + CH_4 + CO_2)$ was 6–24 at 323–473 K. Since the permeation flux in the MTES membrane was affected by both molecular sieving and surface diffusion, high H_2 selectivity could be obtained at elevated temperatures. The transient permeation/separation behaviours of hydrogen multi-component systems on the MTES membrane were predicted by the Generalized Maxwell–Stefan model incorporating the dusty gas model and Langmuir isotherm model.

Keywords: MTES templating; Silica membrane; Hydrogen; Carbon monoxide; Carbon dioxide; Methane

1. Introduction

Hydrogen is considered to be one of the most important chemicals used in the chemical and petroleum industries. Furthermore, hydrogen can be used as a general purpose energy source for space heating, electric power generation, and transportation fuel. These potential uses have resulted in a huge increase in hydrogen demand.

The current emphasis on hydrogen fuel cells has driven the technological development of hydrogen stations to commercialize fuel cells and fuel cell powered vehicles. Generally, hydrogen stations produce hydrogen on-site. The hydrogen production process requires several units, including desulfurizers, reformers, water gas shift reactors, and H_2 separation apparatuses.

However, in addition to hydrogen, the reformate gas produced by the hydrogen production process also contain by-products, such as carbon monoxide. These by-products tend to contaminate the anode catalysts of polymer electrolyte membrane (PEM) fuel cells. The removal of carbon monoxide in the hydrogen stream is a critical yet challenging issue. Many strategies have been applied to facilitate reformate cleaning, including the application of membrane technology [1–4].

In order to be considered practical, hydrogen stations require small to medium sized hydrogen plants, small spatial occupancy, quick installation, and compact modular configurations. Constructing stations that can continuously generate hydrogen can improve efficiency and limit spatial restrictions. In addition, because the temperature of H_2 mixture produced from reaction is high, the separation technology is needed to work well at high temperature conditions. Membrane separation technology is a simple and low-energy method. In particular, ceramic composite membranes have high thermal, chemical, and mechanical stabilities than those of polymeric membranes and thus have been expected to more suitable for high temperature and sever conditions. Therefore, this can be accomplished by performing the separation process using tubular-type inorganic membranes,

* Corresponding author. Tel. +82 2 2123 2762.
E-mail address: leech@yonsei.ac.kr (C.-H. Lee).

0376-7388/$ – see front matter © 2008 Elsevier B.V. All rights reserved.
doi:10.1016/j.memsci.2008.02.001

such as those made from silica or zeolite. Recent transient permeation experiments involving single gases [2] and binary mixtures [1,5] have also raised the possibility of using silica membranes for hydrogen separation.

This study investigated the permeation and separation of reforming gas from natural gas ($H_2/CH_4/CO/CO_2$: 69/3/2/26, vol.%) in tubular-type MTES (methyltriethoxysilane) templating silica/α-alumina composite membrane at transient and steady-state conditions. Since the removal of CO in the reforming gas is quite important, experiments of CO single gas and H_2/CO (50/50, vol.%) binary mixture were performed separately. In order to depict the permeation and separation mechanisms of multi-component theoretically, the GMS (generalized Maxwell–Stefan) model incorporating the DGM (dust gas model) and Langmuir isotherm model were applied to the experimental results.

2. Theory

A quantitative description of mass transfer in porous media must ensure the local conservation of mass for each participating species. In this study, a dynamic model incorporating mass and energy balances were adopted to analyze the permeation mechanism.

2.1. Transient permeation

The mass balance of a component, i, in an infinitesimal volume can be presented as follows [6,7]:

$$\frac{\varepsilon}{RT}\frac{\partial P_i}{\partial t} + (1-\varepsilon)\frac{\partial q_i}{\partial t} = -\frac{1}{r}\frac{\partial (rN_i^{\mathrm{tot}})}{\partial r} \quad (i = 1, \ldots, n) \tag{1}$$

where P_i is the partial pressure, q_i is the adsorbed phase concentration, ε is the porosity and N_i^{tot} is the total molar flux. Eq. (1) states that the local partial pressure and concentration of the adsorbed species change with time, depending on the transport rate of the components.

2.2. Total permeation

The total permeation flux is composed of pore diffusion and surface diffusion:

$$N_i^{\mathrm{tot}} = \left(\frac{\varepsilon}{\tau}\right)\cdot N_i^{\mathrm{P}} + (1-\varepsilon)\cdot N_i^{\mathrm{S}} \tag{2}$$

where N_i^{P} is the flux by pore diffusion, N_i^{S} is the flux by surface diffusion, and τ is the tortuosity factor of the membrane layer.

2.3. Pore diffusion (DGM)

The multi-component macro- or meso-pore diffusion consisting of Knudsen diffusion and Poiseuille diffusion can be expressed by the DGM (Dusty gas model) [6–8].

$$N_i^{\mathrm{P}} = -\frac{\varepsilon}{\tau}\frac{1}{RT}\left(D_i^{\mathrm{Kn}} + \frac{B_i^0}{\eta_i}P_i\right)\cdot\frac{\partial P_i}{\partial r} \tag{3}$$

For a homogeneous porous structure, the pore diffusion contains the two parameters, D_i^{Kn} (Knudsen diffusivity: Eq. (4)) and B_i^0 (viscous diffusion parameter: Eq. (5)). These can be determined by the following equations [9,10]:

$$D_i^{\mathrm{Kn}} = \frac{2r_{\mathrm{P}}}{3}\cdot\sqrt{\frac{8RT}{\pi M_i}} \tag{4}$$

$$B_i^0 = \frac{r_{\mathrm{P}}^2}{8} \tag{5}$$

where r_{P} is the pore radius, R is the ideal gas constant, T is temperature, M is molecular weight, and η_i is the viscosity of each gas [10,11].

2.4. Surface diffusion (generalized Maxwell–Stefan model)

The molar flux by surface diffusion can be calculated by the GMS model combined with surface coverage. The surface fluxes through a membrane in a single (Eq. (6)) and binary (Eq. (7)) systems are described as below:

$$N_1^{\mathrm{S}} = -\rho\cdot(1-\varepsilon)\cdot q_1^{\mathrm{sat}}\cdot\frac{Đ_1^{\mathrm{S}}}{1-\theta_1}\cdot\nabla\theta_1 \quad (i = 1, 2, \ldots, n) \tag{6}$$

$$N_1^{\mathrm{S}} = -\rho\cdot(1-\varepsilon)\cdot q_1^{\mathrm{sat}}\cdot\frac{Đ_1^{\mathrm{S}}}{1-\theta_1-\theta_2}\cdot\frac{[(1-\theta_2)+\theta_1(Đ_2^{\mathrm{S}}/Đ_{12}^{\mathrm{S}})]\nabla\theta_1 + [\theta_1+\theta_1(Đ_2^{\mathrm{S}}/Đ_{12}^{\mathrm{S}})]\nabla\theta_2}{\theta_2(Đ_1^{\mathrm{S}}/Đ_{12}^{\mathrm{S}})+\theta_1(Đ_2^{\mathrm{S}}/Đ_{12}^{\mathrm{S}})+1} \tag{7}$$

A special case of Eq. (7) is that friction between molecules is less important than friction with the wall. In that case, $Đ_{ij}^{\mathrm{S}}$ (=∞) is much higher than $Đ_i^{\mathrm{S}}$, and Eq. (7) is reduced to

$$N_1^{\mathrm{S}} = -\rho\cdot(1-\varepsilon)\cdot q_1^{\mathrm{sat}}\cdot\frac{Đ_1^{\mathrm{S}}}{1-\theta_1-\theta_2}\cdot[(1-\theta_2)\nabla\theta_1+\theta_1\nabla\theta_2] \tag{8}$$

And the surface flux of quaternary mixture can be also described as follows:

$$N_1^{\mathrm{S}} = -\rho(1-\varepsilon)q_{\mathrm{sat}}\frac{Đ_1^{\mathrm{S}}}{1-\theta_1-\theta_2-\theta_3-\theta_4}\times[(1-\theta_2-\theta_3-\theta_4)\nabla\theta_1+\theta_1(\nabla\theta_2+\nabla\theta_3+\nabla\theta_4)] \tag{9}$$

In this study, the surface coverage, θ_i, was calculated by the following Langmuir isotherm model:

$$\theta_i = \frac{q_i}{q_i^{\mathrm{sat}}} = \frac{b_iP_i}{1+\sum_{j=1}^{n}b_jP_j} \tag{10}$$

If molecule–molecule interactions cannot be ignored, Eq. (7) should be used. $Đ_{ij}^{\mathrm{S}}$ from the single component diffusivities can be determined by using the empirical relation [10,11]:

$$Đ_{ij}^{\mathrm{S}} = Đ_i^{\mathrm{S}^{\theta_i/(\theta_i+\theta_j)}}Đ_i^{\mathrm{S}^{\theta_j/(\theta_i+\theta_j)}} \tag{11}$$

The cross-term diffusivities satisfy the Onsager reciprocity relation [10,12]:

$$Đ_{ij}^{S} = Đ_{ji}^{S} \quad (12)$$

2.5. Heat effect

The overall energy balance can be expressed as follows [13,14]:

$$\Delta H_{ads} \cdot A(N_{i,in}^{tot} - N_{i,out}^{tot}) = \rho C_p V \frac{\partial T}{\partial t} + h_i A(T_{in} - T_{out}) \quad (13)$$

where ΔH_{ads} is the heat of adsorption on the membrane, A is the effective membrane area, C_p is the heat capacity, V is the volume of the layer, h_i is the convective heat transfer coefficient of the feed gas and T_{out} is the feed temperature.

2.6. Temperature dependencies on parameters

The change of temperature leads to variation of surface diffusivity and adsorption equilibrium. The temperature dependency of surface diffusivity can be expressed by the following Arrhenius-type relationship [12,15]:

$$Đ_i^{S} = Đ_{0,i}^{S} \exp\left(\frac{-E_D}{RT}\right) \quad (14)$$

where E_D is the diffusional activation energy and $Đ_{0,i}$ is the diffusivity at infinite temperature. The temperature dependency of adsorption parameters, q_i^{sat} and b_i, can be calculated with the LRC (loading ratio correlation) using the Langmuir isotherm [9] and b_i is related to heat of adsorption using the van't Hoff equation [10]

$$q_i^{sat} = \frac{k_1}{T^{k_2}} \quad (15)$$

$$b_i = b_{i,0} \exp\left(\frac{\Delta H_{ads}}{RT}\right) \quad (16)$$

where k_1 and k_2 are the fitting parameters and $b_{i,0}$ is the Langmuir parameter at zero loading.

3. Experimental

3.1. Membrane preparation

A MTES sol as the structure-directing agent was used for the templating material in the fabrication of a nano-porous silica/α-alumina composite membrane. The SiO_2/α-Al_2O_3 composite support (1.6 nm mean pore diameter) was prepared using a pressurized coating of colloidal silica sol inside the tubular α-Al_2O_3 supports (7.8 mm outside diameter, 6.2 mm inside diameter, 0.8 mm thickness, 100 mm length, and 0.1 μm mean pore diameter). The organic templating silica sol was prepared from the mixture of silica sol and organic template MTES. The organic templating silica composite membrane was then fabricated by dip-coating the SiO_2/α-Al_2O_3 composite supports in the templating silica sols. The whole process of dip-coating, drying, and calcining was repeated several times to repair any defects in the silica layer. The pore size of the silica composite membrane was controlled using the TEOS-EtOH solution. In this study, to identify the mechanical strength of the membrane, the burst strength of the membrane was measured by using the hydraulic pressure (water at room temperature) of 10 $kg_f\,cm^{-2}$, under which condition the membrane showed no damage. The synthesis and characteristics of the membrane have previously been described in detail [5,16,17]

3.2. Permeation experiments

The permeation experiments in the inorganic membranes were performed at temperatures between 323 and 473 K and pressures of 100–600 kPa The permeation experiments of pure gas (CO, 99.99% purity) were measured in dead-end mode without the retentate stream, and the permeation/separation experiments of binary (H_2/CO, 50/50, vol.%) and quaternary (H_2/CH_4/CO/CO_2, 69/3/2/26, vol.%) mixtures were measured in stage-cut mode by controlling feed and retentate flow rates. The permeation flux and composition were measured using a mass flow meter and an online quadrupole mass spectrometer (QMG 422, Balzers Co., Germany). Experiments involving a depressurization (DP, feed pressure → atmospheric pressure) step and a pressurization (PR, atmospheric pressure → feed pressure) step were performed to investigate permeation/separation mechanism. In general, the pores in inorganic membranes become occupied by contaminating molecules due to their adsorption at low temperature, resulting in the hindrance of permeation of desired molecules. In order to alleviate this problem, a backwashing (DP) step was added to the experimental process. In addition, the permeation mechanism can be confirmed by DP experimental results. The detailed experimental system and the permeation measurement procedure were described in a previous study [2,5].

3.3. Numerical simulation

In this study, the gPROMS modeling tool (Process Systems Enterprise Ltd.) was used to obtain the solution of dynamic simulation from the mathematical model mentioned above. A centered finite difference method (CFDM) of the second order was applied to the spatial partial derivatives. The DAEs (differential-algebraic equations) for temporal domain were subsequently integrated by employing an integrator, called DASOLV, included in the gPROMS library. The results of numerical simulation were stable for the range of conditions used in this study.

4. Results and discussion

4.1. Transient permeations of pure CO: pressure and temperature effect

Since CO acts as a poison for fuel cells, it is important to remove CO from reforming gas before use. Elucidating the permeation mechanisms of pure CO is needed in order to understand

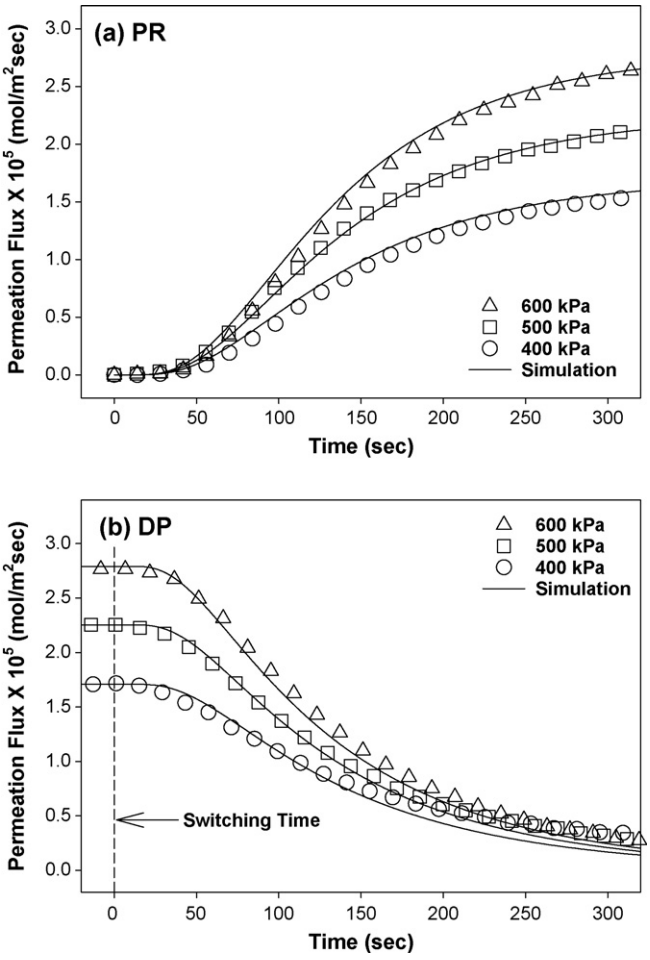

Fig. 1. Pressure effect of transient permeation flux of CO on a MTES templating silica/α-alumina composite membrane: (a) PR step and (b) DP step at 373 K: dead end (stage cut = 1) and sweeping gas (flow rate = 0.68×10^{-6} $m^3 s^{-1}$) condition.

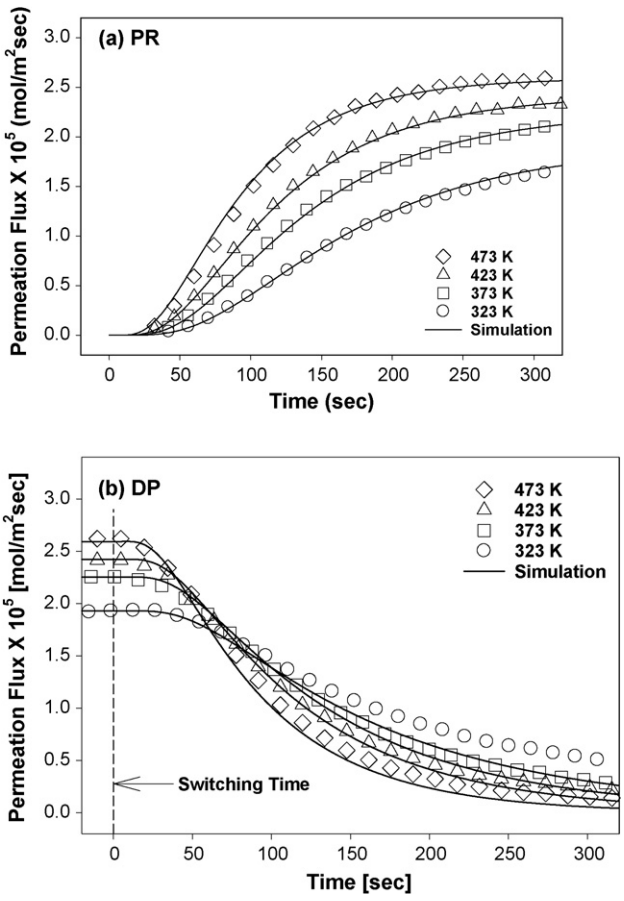

Fig. 2. Temperature effect of transient permeation flux of CO on a MTES templating silica/α-alumina composite membrane: (a) PR step and (b) DP step at 500 kPa: dead end (stage cut = 1) and sweeping gas (flow rate = 0.68×10^{-6} $m^3 s^{-1}$) condition.

the process by which hydrogen is separated from natural gas. Fig. 1 shows the effect of pressure on transient permeation flux of CO at 373 K. Increased pressure caused the occupancy of CO on the membrane layer to increase and the time to reach the steady state to decrease slightly. This is because the chemical potential gradient of the adsorbed phase decreases as coverage approaches saturation at higher pressure. In addition, the time to reach the steady state of desorption in MTES membrane was similar at all pressure ranges during the depressurization (DP) step (Fig. 1b).

Temperature changes can also have a great influence on CO permeation behavior. Fig. 2 shows the effect of temperature on transient permeation flux of CO at 500 kPa. As shown in Fig. 2, the time required to reach steady-state flux at both PR and DP steps decreased with increasing temperature due to the activation of molecules [2]. Moreover, as shown in Fig. 2b, the desorption rate at the DP step became faster at higher temperature in the adsorptive porous membrane layer. Therefore, the transient permeation flux curves at low and high temperatures crossed during the time interval between 50 and 100 s.

4.2. Comparison of steady-state permeation of pure CO to other molecules

Fig. 3 shows the steady-state fluxes of pure gases at feed pressure and temperature under dead end condition. The permeance

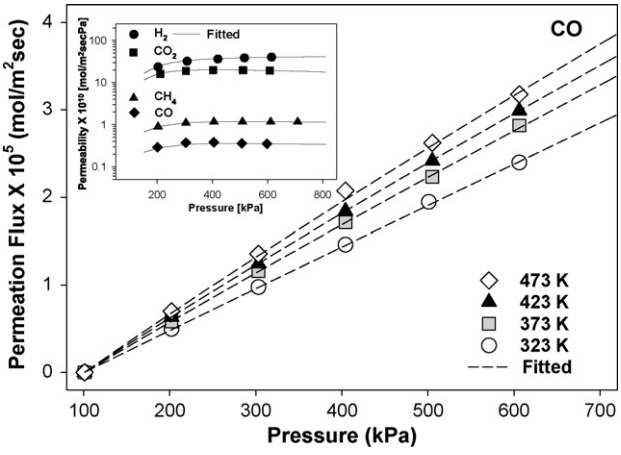

Fig. 3. Permeation flux of pure CO on a MTES templating silica/α-alumina composite membrane at 323–473 K and referenced permeabilities of H_2, CO_2, CH_4 and CO pure gases at 473 K: dead end (stage cut = 1) and sweeping gas (flow rate = 0.68×10^{-6} $m^3 s^{-1}$) condition.

and permselectivity of single gas in the templating membrane were discussed in the previous study in terms of pore and membrane structure, molecular size and adsorption affinity [2]. In this study, the CO results in the membrane were compared to the characteristics of the other single gases. The permeation fluxes of CO were linearly proportional to feed pressure, which is similar to the permeation flux of H_2 on the MTES membrane. CO_2 and CH_4 both have strong adsorption affinities on the membrane and favorable permeation flux curvatures [2]. Therefore, CO is presumed to be a weak adsorbate. In addition, the increase in permeate flux of CO with rising temperature is similar to the results with H_2 and CH_4 and different from the results with CO_2 [2]. Therefore, the diffusional mechanism of CO in the membrane is presumed to be similar to that of H_2 and CH_4.

Using steady-state permeation flux (Eq. (2)) in Fig. 3 and transient permeation flux (Eq. (1)) in Figs. 1 and 2, the single gas transport parameters, such as Maxwell–Stefan diffusivity (Eq. (6)), Langmuir parameter and saturated amount of adsorption (Eq. (10)), were estimated with the gPROMS estimation tool. As shown in Figs. 1–3, the simulated results for the PR and DP steps agreed well with the experimental results, including the steady-state and transient permeation behaviors. The obtained values and permeabilities of each gas are presented in Table 1.

Table 1 and Fig. 3 demonstrate that the permeance of H_2 and CO_2 was higher than the others. Increased permeance of H_2 was ascribed to its small molecular size and the increased permeance of CO_2 was ascribed to its high surface diffusion [2]. However, the permeance of CO on the MTES membrane was much lower (CO ≈ 4.79–6.46×10^{-11} mol m^{-2} s^{-1} Pa^{-1}) than that of the other molecules. It is noteworthy that the diffusivity of CH_4 is slightly lower than that of CO (Table 1), even though the permeance of CH_4 is far higher than that of CO. This may be due to differences in molecular structure between CH_4 and CO. While CO has a linear structure, CH_4 has a tetrahedral molecular structure which might adversely affect diffusion due to steric hindrance. On the contrary, the contribution of surface diffusion to permeance is higher for CH_4 than for CO, owing to the stronger adsorption affinity of CH_4.

4.3. Transient permeation and separation of H_2/CO binary system

The permeation flux and separation factor of the H_2/CO (50:50, vol.%) binary mixture were measured as functions of pressure and temperature. Fig. 4a shows the transient permeation curves of the H_2/CO mixture at 373 K and 600 kPa at the PR step. H_2 molecules started to permeate the membrane within 10 s; however, only minor permeation of CO was observed after 50 s. The permeation flux of H_2 reached plateau (steady state) at about 150 s while that of CO reached plateau at about 250 s.

The experiments using single gases showed that the permeation flux of H_2 reached steady state within 30 s [2] while that of CO took over 500 s to reach steady state. However, comparison of Fig. 4a to Figs. 1 and 2 reveals that the permeation flux rate of CO in the H_2/CO mixture increased while that of H_2 decreased. H_2 permeation was inhibited by CO molecules that had become stagnated after being adsorbed into membrane pores. In contrast, CO permeation was enhanced by H_2 permeation. Similar phenomena were also observed in other H_2 binary systems [1].

Fig. 4b demonstrates that the simulated results for the CO transient curve at the DP step agreed well with experimental data in spite of using estimated parameters from PR step transient curve. On the contrary, the transient permeation behavior of H_2 at the DP step differed significantly from the result at the PR step. This resulted in a large deviation between simulated and experimental results in permeation flux and separation fac-

Table 1
Permeance, diffusivity, saturated amount of adsorption and Langmuir parameter of H_2, CH_4, CO, and CO_2 on MTES membrane

	Permeance (mol m^{-2} s^{-1} Pa^{-1})	$Đ_1^S$ (m^2 s^{-1})	q_{sat} (mol g^{-1})	b (Pa^{-1})
H_2				
323 K	2.89×10^{-9}	8.50×10^{-11}[a]	9.60×10^{-3}[a]	2.30×10^{-7}[a]
373 K	4.79×10^{-9}	1.97×10^{-10}[a]	8.05×10^{-3}[a]	1.96×10^{-7}[a]
423 K	6.11×10^{-9}	2.60×10^{-10}[a]	7.92×10^{-3}[a]	1.94×10^{-7}[a]
473 K	6.62×10^{-9}	2.81×10^{-10}[a]	7.90×10^{-3}[a]	1.93×10^{-7}[a]
CH_4				
323 K	1.20×10^{-10}	1.27×10^{-12}[a]	1.60×10^{-3}[a]	6.10×10^{-6}[a]
373 K	1.29×10^{-10}	1.88×10^{-12}[a]	1.43×10^{-3}[a]	4.90×10^{-6}[a]
423 K	1.39×10^{-10}	2.60×10^{-12}[a]	1.30×10^{-3}[a]	4.05×10^{-6}[a]
473 K	1.45×10^{-10}	2.95×10^{-12}[a]	1.28×10^{-3}[a]	3.90×10^{-6}[a]
CO				
323 K	4.79×10^{-11}	1.46×10^{-12}[a]	4.20×10^{-4}[a]	1.10×10^{-6}
373 K	5.58×10^{-11}	3.50×10^{-12}[a]	4.15×10^{-4}[a]	1.08×10^{-6}
423 K	5.97×10^{-11}	5.10×10^{-12}[a]	4.05×10^{-4}[a]	1.00×10^{-6}
473 K	6.46×10^{-11}	7.70×10^{-12}[a]	3.90×10^{-4}[a]	8.20×10^{-7}
CO_2				
323 K	3.05×10^{-9}	1.69×10^{-11}[a]	5.12×10^{-3}[a]	6.11×10^{-6}[a]
373 K	2.46×10^{-9}	3.10×10^{-11}[a]	2.60×10^{-3}[a]	4.00×10^{-6}[a]
423 K	2.00×10^{-9}	3.60×10^{-11}[a]	1.94×10^{-3}[a]	3.45×10^{-6}[a]
473 K	1.50×10^{-9}	4.21×10^{-11}[a]	1.37×10^{-3}[a]	3.11×10^{-6}[a]

[a] Referred from Moon et al. [2].

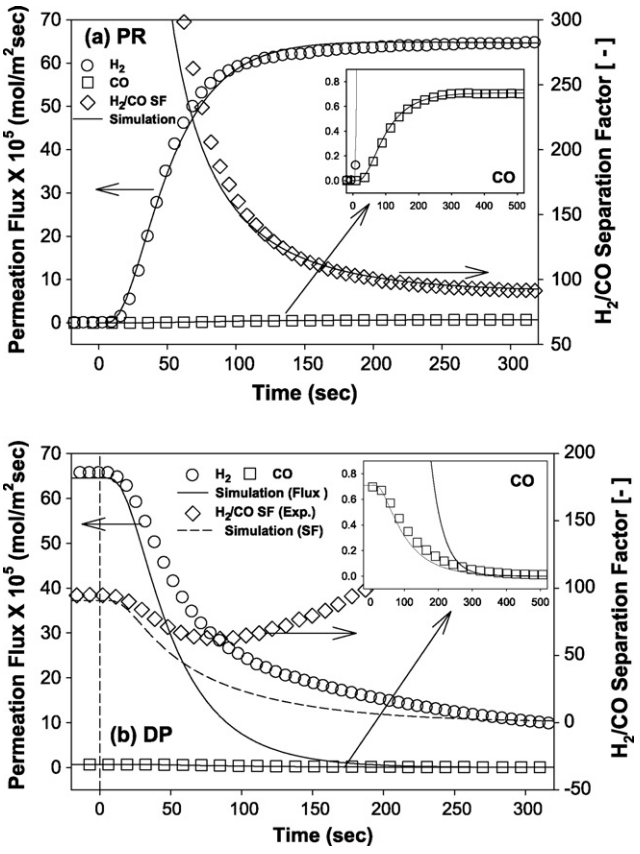

Fig. 4. Transient permeation flux in H_2/CO binary mixture (50/50, vol.%) on a MTES templating silica/α-alumina composite membrane at 323 K and 500 kPa: (a) PR (pressurization) step and (b) DP (depressurization) step. Sweeping gas flow rate (=0.85×10^{-6} $m^3 s^{-1}$) and stage cut (=0.60) were maintained constantly.

tor. As shown in Fig. 4b, the permeation flux of H_2 decreased drastically at the beginning of the DP step. However, the tailing phenomenon was observed after 100 s because H_2 molecules with small kinetic diameter and low adsorption affinity (Table 1) remain in the pore under near atmospheric condition.

Fig. 5 shows temperature dependencies of transient permeation flux and separation factor of H_2/CO mixture (50/50, vol.%) and Table 2 shows the permeance and diffusivity estimated from experimental data on the MTES membrane at various temperatures and fixed pressure (500 kPa). As shown in Fig. 5 and Table 2, permeance and diffusivity of CO in the H_2/CO binary system were increased with temperature. In addition, both the permeation flux and rate to reach steady state increased with temperature. This is because both H_2 and CO are weak-adsorptive

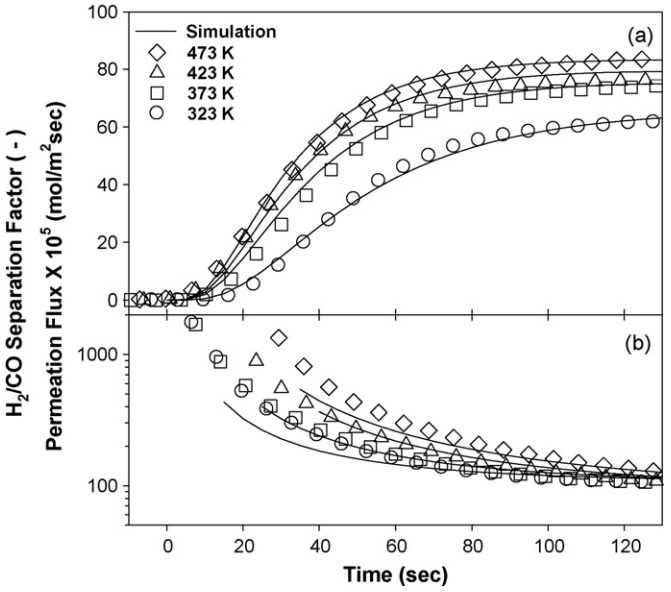

Fig. 5. Temperature dependencies of transient permeation flux of H_2/CO binary mixture (50/50, vol.%) on a MTES templating silica/α-alumina composite membrane at 500 kPa: (a) H_2/CO binary mixture permeation fluxes and (b) H_2/CO separation factor. Sweeping gas flow rate (=0.85×10^{-6} $m^3 s^{-1}$) and stage cut (=0.60) were maintained constantly.

molecules and their molecular movements are activated with temperature. The shape of the transient permeation flux curve of CO changed was significantly when the temperature was raised from 323 to 373 K, which was similar to the results with pure CO in Fig. 2a. Unlike transient permeation flux behaviors, the H_2/CO separation factors (flux ratio between H_2 and CO) were not significantly affected by temperature, except for at the initial onset of the experiment (Fig. 5b).

4.4. Steady-state permeation and separation of H_2/CO binary system

Fig. 6 shows the steady-state permeation flux curve and separation factor of the H_2/CO mixture in the range of 323–473 K. The steady-state permeation flux of H_2/CO mixture was almost linearly proportional to feed pressure. The average permeance and separation factor were 1.53–2.04×10^{-9} mol m^{-2} s^{-1} Pa^{-1} and 92.99–110.40, respectively.

Due to increased mobility of the molecules in the MTES membrane pores, the permeation flux of H_2/CO mixture increased with temperature (Fig. 6a). The separation factor of H_2/CO mixture increased with temperature at a fixed pressure,

Table 2
The permeance and Maxwell–Stefan diffusivity of H_2/CO mixture

	Permeance (mol m^{-2} s^{-1} Pa^{-1})			$Đ_1^S$ (m^2 s^{-1})	
	H_2/CO	H_2	CO	H_2	CO
323 K	1.53×10^{-9}	1.51×10^{-9}	1.63×10^{-11}	2.70×10^{-11}	4.60×10^{-12}
373 K	1.83×10^{-9}	1.81×10^{-9}	1.73×10^{-11}	3.75×10^{-11}	8.20×10^{-12}
423 K	1.98×10^{-9}	1.96×10^{-9}	1.85×10^{-11}	4.08×10^{-11}	1.16×10^{-11}
473 K	2.04×10^{-9}	2.02×10^{-9}	1.83×10^{-11}	4.40×10^{-11}	1.60×10^{-11}

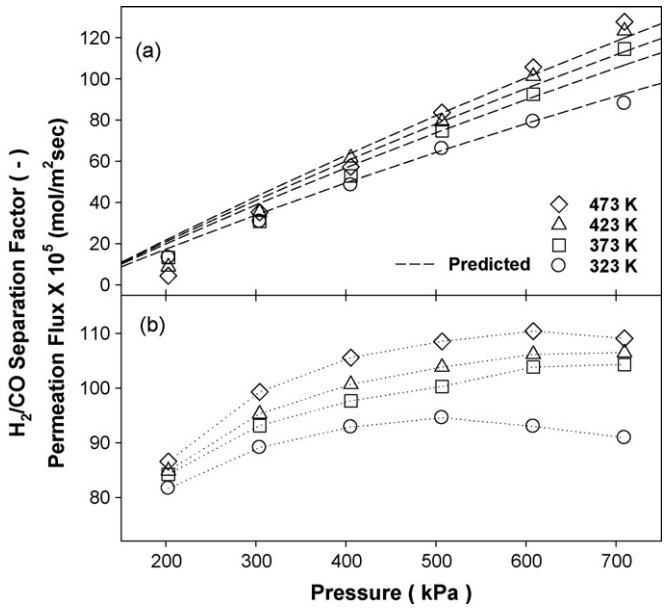

Fig. 6. Steady-state permeation of H_2/CO binary mixture (50/50, vol.%) on a MTES templating silica/α-alumina composite membrane at 323–473 K: (a) H_2/CO binary mixture permeation fluxes and (b) H_2/CO separation factor. Sweeping gas flow rate (=0.85 × 10^{-6} m^3s^{-1}) and stage cut (=0.60), were maintained constantly.

and also increased slightly with pressure at a fixed temperature (Fig. 6b). Fig. 3 indicates that the permeation flux of pure CO increased almost linearly with pressure; however the increasing ratio of CO permeation flux was much smaller than that of H_2 [2]. As a result, the H_2/CO separation factor did not increase linearly with pressure. Except for 323 K, the separation factor at each temperature was converged between 100 and 110 with an increase in pressure. Since CO molecules are weakly adsorbed on the pore wall compared to the other adsorptive molecules, such as CO_2 and CH_4, H_2 permeation is less disturbed by CO. Therefore, in the H_2/CO system, higher separation factors could be expected than those in the H_2/CO_2 and H_2/CH_4 systems [1]. As shown in Table 3, the permselectivity calculated from single gas permeation was different from the separation factor obtained from binary separation. However, since the permeation mechanisms of H_2 and CO are dominated by molecular sieving rather than surface diffusion, especially at higher temperature, the permselectivity became similar to the separation factor. In addition, the separation factor increased relative to temperature in all the binary systems.

Table 3
The permselectivities and separation factors of H_2/CH_4, H_2/CO, H_2/CO_2 binary mixtures (50/50, vol.%) at 600 kPa and 323–473 K temperature range

	H_2/CH_4[a]	H_2/CO	H_2/CO_2[a]
Permselectivity			
323 K	24.01	61.39	0.99
373 K	36.58	86.97	2.08
423 K	43.24	103.60	3.28
473 K	44.18	103.59	4.48
Separation factor			
323 K	10.49	92.99	1.68
373 K	16.17	104.83	3.00
423 K	18.64	106.16	4.36
473 K	20.74	110.40	6.45

[a] Referred from Moon et al. [1].

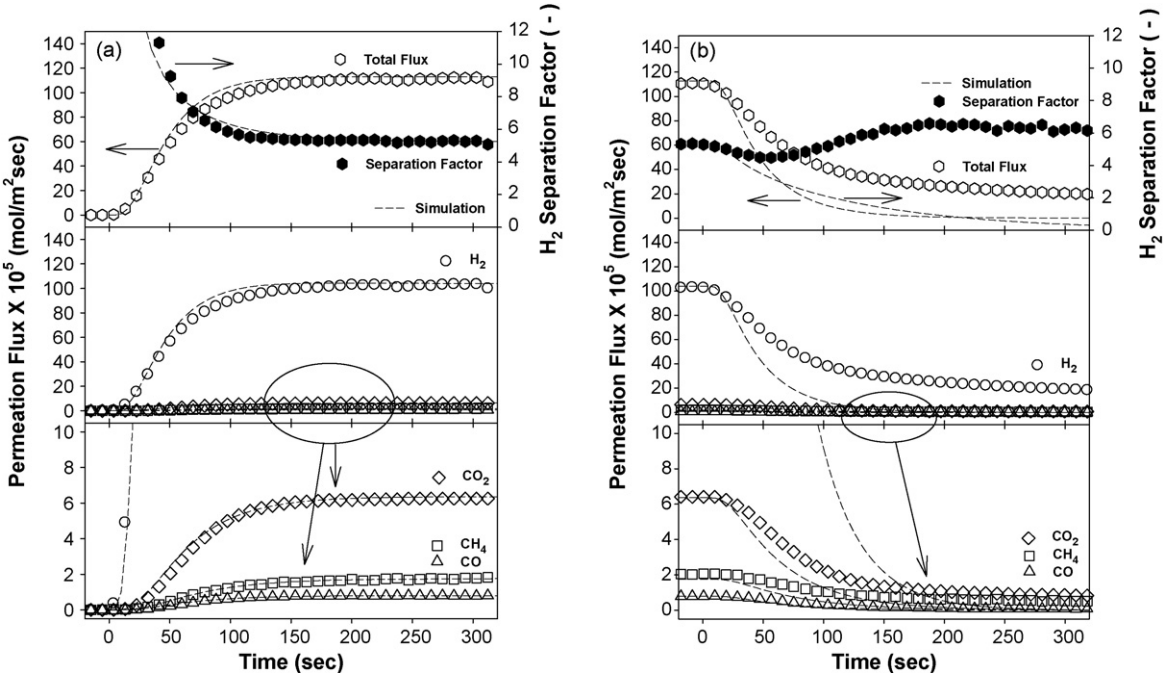

Fig. 7. Transient permeation flux and separation factor of $H_2/CH_4/CO/CO_2$ quaternary mixture (69/3/2/26, vol.%) at (a) PR step and (b) DP step on a MTES templating silica/α-alumina composite membrane at 373 K and 600 kPa: top) total flux and H_2 separation factor, middle and bottom) transient permeation of each gases. Sweeping gas flow rate (=0.85 × 10^{-6} m^3s^{-1}) and stage cut (=0.60) were maintained constantly.

4.5. Transient permeation and separation of quaternary mixture

Fig. 7 shows the transient permeation and separation factor curves for the $H_2/CH_4/CO/CO_2$ quaternary mixture (69/3/2/26, vol.%) at 373 K and 600 kPa (500 kPa pressure drop). The composition of quaternary mixture used in this study was similar to the actual gas mixture produced using a hydrogen reformer on natural gas.

Fig. 7a demonstrates that, during the PR step, transient permeation of H_2 molecules started within 10 s while permeation of other components was observed after 10–20 s. Initially, little permeation was observed due to the competitive adsorption and pore filling that occurred in the silica layer of the membrane. After a certain period of time, CO_2, CH_4 and CO began to permeate the membrane in sequence. Unlike the adsorptive molecules through the zeolite- or CMS-type membrane [1,2], the roll-up phenomenon was not observed in the transient permeation profiles in spite of the weak adsorption of H_2 and strong adsorption of CO_2 or CH_4 in the membrane pores. As the adsorption process proceeded, the vacant sites in the pore were mainly occupied by CO_2. This is because of the strong adsorption affinity and high partial pressure of CO_2 in the feed. Therefore, the surface concentration of CO and CH_4 with lower diffusivity and H_2 with weak adsorption affinity could not be intensified to show the roll-up. Furthermore, Fig. 7a showed that CO could be removed most effectively from the feed gas in the MTES membrane due to the higher adsorption affinity and hindrance effect of CO_2 and CH_4.

Fig. 7b shows the transient permeation flux of H_2 quaternary mixture at the DP step. The sequence to reach the completely desorbed (regenerated) state of each component is the same as the results at the PR step in Fig. 8a. In this study, both diffusivity difference and competitive adsorption between molecules work as a driving force of permeation and separation. As shown in Fig. 7a, the transient simulated results at the PR step were well fitted to the experimental data. However, in the case of the DP step, some deviations in the transient curves of H_2 and CO_2 were observed between the simulated results and experimental data in Fig. 7b when the parameters obtained at the PR step were applied. This implies that the mechanism at the PR step is different from that at the DP step.

Similar to the phenomenon observed with the H_2/CO binary mixture, the permeation flux of H_2 at the beginning of the DP step decreased drastically. Since H_2 permeation is mainly affected by pore diffusion or molecular sieving rather than by surface diffusion, the diminished pressure drop at the DP step was not a significant driving force for H_2 permeation. In addition, because surface diffusion is the dominant transport mechanism of CO_2 on the MTES membrane, concentration gradient is more important than pressure difference for driving membrane transport. Therefore, the permeation flux of these molecules decreased drastically over time. Moreover, the tailing phenomenon in the quaternary mixture was observed after 100 s, which was the same as the result with the H_2/CO binary mixture in Fig. 4. At the DP step, H_2 with low adsorption affinity remained in the pore and the permeation was disturbed by the other gases when the pressure approached atmospheric conditions., particularly by CO_2 and partially CH_4,. However, it is noted that the permeation flux of CO reaches to zero concentration without any tailing at the DP step. Therefore, it is confirmed that CO molecules are very weakly adsorbed in the membrane pore at the PR step as mentioned above.

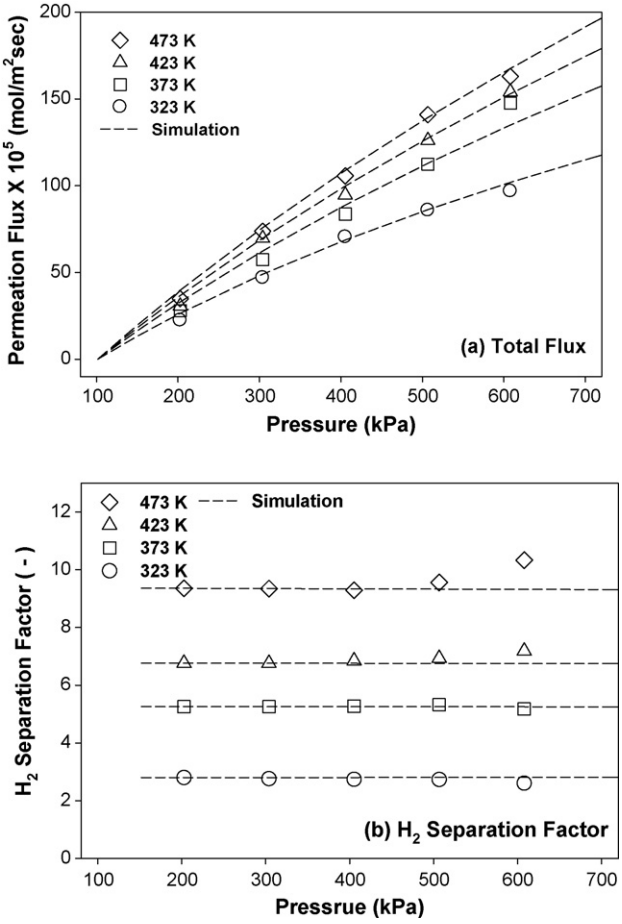

Fig. 8. Steady-state permeation of $H_2/CH_4/CO/CO_2$ quaternary mixture (69/3/2/26 vol.%) on a MTES templating silica/α-alumina composite membrane at 323–473 K: (a) permeation flux and (b) H_2 separation factor. Sweeping gas flow rate ($=0.85 \times 10^{-6}\ m^3 s^{-1}$) and stage cut (=0.60) were maintained constantly.

4.6. Steady-state permeation and separation of $H_2/CH_4/CO/CO_2$ quaternary mixture

Fig. 8 shows the steady-state permeation and separation factor of $H_2/CH_4/CO/CO_2$ quaternary mixture (69/3/2/26, vol.%) through the MTES membrane. The permeation flux of the quaternary mixture became almost linearly proportional to feed pressure with an increase in temperature, whereas the separation factor variation was comparatively small with feed pressure. The separation factor could be improved by increasing temperature at the pressure range tested. The permeance of the quaternary mixture on the MTES membrane is $2.07–3.37 \times 10^{-9}\ mol\ m^{-2}\ s^{-1}\ Pa^{-1}$ and the separation factor of $H_2/(CH_4 + CO + CO_2)$ is 2.61–10.33 (Table 4).

Table 4
Permeance and separation factor of quaternary mixture ($H_2/CH_4/CO/CO_2$: 69/3/2/26, vol.%)

	Permeance (mol m^{-2} s^{-1} Pa^{-1})	Permselectivity	Separation factor
323 K	2.07×10^{-9}	1.12	2.61
373 K	2.84×10^{-9}	2.30	5.18
423 K	3.10×10^{-9}	3.61	7.18
473 K	3.37×10^{-9}	5.19	10.33

In the quaternary mixture, the feed stream was mainly composed of H_2 and CO_2. In addition, as shown in Table 1, single gas permeabilities of CH_4 and CO on MTES membranes are far lower than those of H_2 and CO_2. The permselectivity and separation factor of the H_2/CO_2 mixture are far lower than those of the other binary mixtures due to the strong adsorption affinity and fast surface diffusion of CO_2 [1]. In addition, CH_4 and CO played relatively minor roles in the quaternary mixture permeation/separation behaviors owing to their weak adsorption affinity and slow diffusion. Therefore, the permeation behavior of the quaternary mixture was similar to that of the H_2/CO_2 mixture. Moreover, as shown in Table 4, the separation factor at each temperature was approximately two-fold higher than the permselectivity. This implies that molecular interactions contribute to the permeation and separation of the quaternary mixture on the METS membrane.

Fig. 9 shows the steady-state permeation of each component ((a) H_2, (b) CH_4, (c) CO, and (d) CO_2 in $H_2/CH_4/CO/CO_2$ quaternary mixture (69/3/2/26, vol.%)) at 473K on the MTES membrane. In the quaternary mixture, H_2 was found to have almost linear permeation flux relative to increasing feed pressure. On the contrary, CO_2 permeation flux exhibited a favorable curvature. The permeation fluxes of CH_4 and CO were linear with respect to changes in pressure; however, the CH_4 and CO permeation fluxes varied only slightly compared to those of H_2 and CO_2.

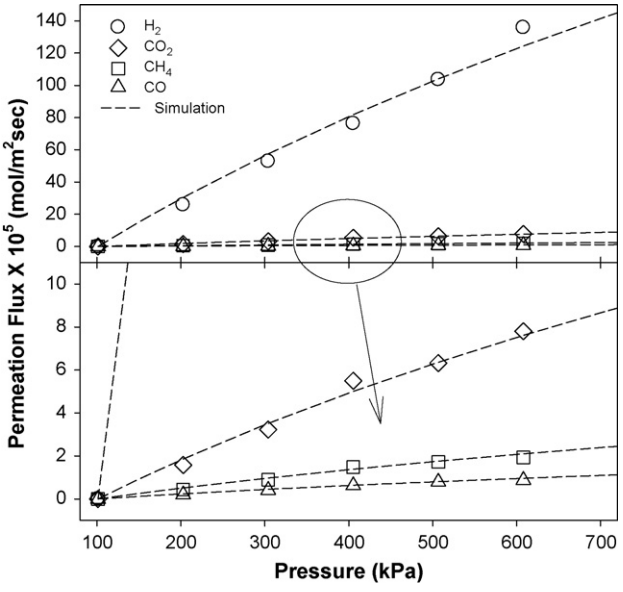

Fig. 9. Steady-state permeation of each component in $H_2/CH_4/CO/CO_2$ quaternary mixture (69/3/2/26, vol.%) on a MTES templating silica/α-alumina composite membrane at 373 K: Sweeping gas flow rate (=0.85×10^{-6} m^{3}s^{-1}) and stage cut (=0.60), were maintained constantly.

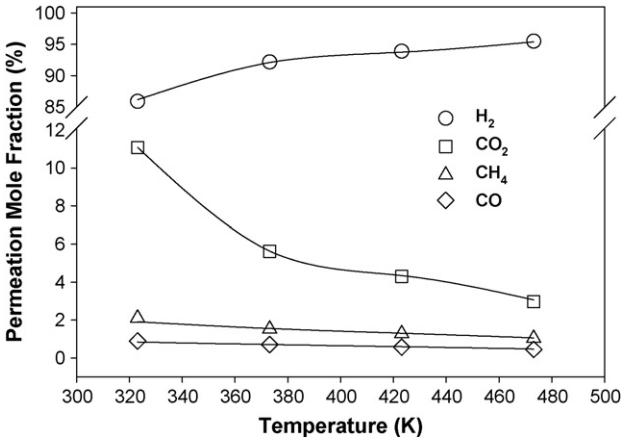

Fig. 10. Temperature dependency of permeation mole fraction of $H_2/CH_4/CO/CO_2$ quaternary mixture (69/3/2/26, vol.%) on a MTES templating silica/α-alumina composite membrane at 500 kPa and 323–473 K. Sweeping gas flow rate (=0.85×10^{-6} m^{3}s^{-1}) and stage cut (=0.60) were maintained constantly.

Fig. 10 shows the temperature dependency of permeation mole fraction of $H_2/CH_4/CO/CO_2$ mixture. At low temperature, due to the fast surface diffusion and strong adsorption of CO_2, the permeation of H_2 was significantly hindered by the preoccupied CO_2 in the pore wall of the membrane. Therefore, the low H_2 selectivity was observed in Fig. 8 and the permeation mole fraction of CO_2 was relatively high in Fig. 10. On the contrary, at high temperature, owing to activation of H_2 molecules and unfavorable adsorptive condition of CO_2 in the membrane pores, the permeation flux of H_2 steeply increased whereas that of CO_2 decreased, as mentioned for single gas permeation.

The temperature dependencies of CO and CH_4 in the quaternary mixture are smaller than H_2 and CO_2. In addition, CO_2 with high partial pressure in the membrane pore leads to hindrance effect for these molecules, even at high temperature. As a result, although the permeation flux of pure CO and CH_4 was increased with temperature, the permeated mole fraction of both molecules in the mixture was slightly decreased, as shown in Fig. 10.

5. Conclusions

Since permeance of pure CO on the MTES membrane is very low (CO ≈ 4.79–6.46 × 10^{-11} mol m^{-2} s^{-1} Pa^{-1}), a high separation factor (92.99–110.40) and permeance (1.53–2.04 × 10^{-9} mol m^{-2} s^{-1} Pa^{-1}) could be obtained from the H_2/CO binary mixture. The MTES membrane has good potential for application in CO clean-up processes for the fuel cell systems and for use in hydrogen stations. In this study, we were able to develop a membrane process suitable for separating H_2 from CO and other reformate gases (CO_2 or CH_4) that showed a molecular sieving effect.

Permeance of the quaternary mixture ($H_2/CH_4/CO/CO_2$) on MTES membrane is 2.07–3.37 × 10^{-9} mol m^{-2} s^{-1} Pa^{-1} and the separation factor of $H_2/(CO + CH_4 + CO_2)$ is 6–24. When the feed pressure was increased, the permeation flux and the

H_2 separation factor increased slightly. Increased temperature caused the permeation flux of H_2 to increase and that of CO_2 to decrease drastically. At low temperature the permeation of H_2 was significantly hindered and low H_2 selectivity was obtained. This was due to the strong surface diffusion effect of CO_2. On the contrary, the permeation and selectivity of H_2 were increased with temperature because of activation of H_2 molecules and unfavorable conditions for CO_2 adsorption. However, because CO and CH_4 showed weak adsorption affinity and slow diffusion on the MTES membrane, their permeation fluxes decreased with an increase in temperature, which was the opposite of what was observed during single gas permeation. Moreover, compared to the other impurities, CO was most successfully removed from the H_2 mixture.

The MTES membrane showed great potential for hydrogen separation from reforming gas with high selectivity and high permeance. Silica membranes are expected to be used for separating hydrogen in reforming environment at high temperatures.

Acknowledgment

This research was supported by the Seoul R&BD Program.

Nomenclature

Roman letters

b_i	parameter in the Langmuir isotherm model (Pa^{-1})
$b_{0,i}$	parameter of species i in the Langmuir isotherm model at zero loading (Pa^{-1})
B_i^0	Poiseuille structural parameters of species i (m^2)
D_i^{Kn}	Knudsen diffusivity of species i ($m^2\ s^{-1}$)
$Đ_{0,i}$	Maxwell–Stefan surface diffusivity at infinite temperature ($m^2\ s^{-1}$)
$Đ_i$	Maxwell–Stefan surface diffusivity ($m^2\ s^{-1}$)
E_a	activation energy ($J\ mol^{-1}$)
ΔH_{ads}	heat of adsorption ($J\ mol^{-1}$)
k_1	temperature dependant parameter for saturated adsorption capacity (mol/g)
k_2	temperature dependant parameter for saturated adsorption capacity
M_i	molecular weight of species i ($mol\ g^{-1}$)
N_i	molar flux of species i ($mol\ m^{-2}\ s^{-1}$)
N_i^P	molar flux of pore diffusion of species i ($mol\ m^{-2}\ s^{-1}$)
N_i^S	molar flux of surface diffusion of species i ($mol\ m^{-2}\ s^{-1}$)
N_i^{tot}	total molar flux of species of i ($mol\ m^{-2}\ s^{-1}$)
P_i	partial pressure of species i (Pa)
q_i	adsorbed species concentration within layer pores ($mol\ g^{-1}$)
${q_i}^{sat}$	saturated capacity of adsorbed species i ($mol\ g^{-1}$)
r_P	pore radius (m)
R	gas constant, 8.314 ($J\ mol^{-1}\ K^{-1}$)
t	time (s)
T	absolute temperature (K)

Greek letters

ε	porosity of membrane
Γ_{ij}	thermodynamic factor of species i,j
η_i	viscosity of species i (Pa s)
μ_i	chemical potential of species I ($J\ mol^{-1}$)
θ_i	fractional surface occupancy of species i
ρ	membrane density ($g\ m^{-3}$)
τ	tortuosity factor

Subscripts/superscripts

i,j,1,2	component i,j,1,2
vis	viscous flow
Kn	Knudsen flow
tot	total flow
sat	saturated

References

[1] J.H. Moon, C.H. Lee, Hydrogen separation characteristics of methyltriethoxysilane templating silica membrane, AIChE J. 53 (12) (2007) 3125.
[2] J.H. Moon, Y.S. Bae, S.H. Hyun, C.H. Lee, Equilibrium and kinetic characteristics of five single gases in a methyltriethoxysilane templating silica/α-alumina composite membrane, J. Membr. Sci. 285 (2006) 343.
[3] M.C. Duke, J.C. Diniz da Costa, G.Q. Lu, P.G. Gray, Modeling hydrogen separation in high temperature silica membrane systems, AIChE J. 52 (5) (2006) 1729.
[4] Y.S. Bae, M.B. Kim, H.J. Lee, C.H. Lee, Adsorptive denitrogenation of light gas oil by silica-zirconia cogel, AIChE J. 52 (2) (2006) 510.
[5] J.H. Moon, Y.J. Park, M.B. Kim, S.H. Hyun, C.H. Lee, Permeation and separation of a carbon dioxide/nitrogen mixture in a methyltriethoxysilane templating silica/α-alumina composite membrane, J. Membr. Sci. 250 (2005) 195.
[6] F. Kapteijn, J.M. van de Graaf, J.A. Moulijn, One-component permeation maximum: diagnostic tool for silicalite-1 membranes, AIChE J. 46 (5) (2000) 1096.
[7] Y.D. Chen, R.T. Yang, Preparation of carbon molecular sieve membrane and diffusion of binary mixtures in the membrane, Ind. Eng. Chem. Res. 33 (1994) 3146.
[8] G. Xomeritakis, S. Naik, C.M. Braunbarth, C.J. Cornelius, R. Pardey, C.J. Brinker, Organic-templated silica membranes: I. Gas and vapor transport properties, J. Membr. Sci. 215 (2003) 225.
[9] H. Ahn, J.H. Moon, S.H. Hyun, C.H. Lee, Diffusion mechanism of carbon dioxide in zeolite 4A and CaX pellets, Adsorption 10 (2004) 111.
[10] J. Karger, D.M. Ruthven, Diffusion in Zeolites and Other Microporous Solids, John Wiley & Sons, 1992.
[11] R.T. Yang, Gas Separation by Adsorption Processes, Butterworths, New York, 1987.
[12] T.Q. Gardner, A.I. Flores, R.D. Noble, J.L. Falconer, Transient measurements of adsorption and diffusion in H-ZSM-5 membranes, AIChE J. 48 (2002) 1155.
[13] J.C. Poshusta, R.D. Noble, J.L. Falconer, Temperature and pressure effects on CO_2 and CH_4 permeation through MFI zeolite membranes, J. Membr. Sci. 160 (1999) 115.
[14] R. Wang, S.L. Liu, T.T. Lin, T.S. Chung, Characterization of hollow fiber membranes in a permeator using binary gas mixtures, Chem. Eng. Sci. 57 (2002) 967.

[15] T.Q. Gardner, J.L. Falconer, R.D. Noble, M.M.P. Zieverink, Analysis of transient permeation fluxes into and out of membrane for adsorption measurements, Chem. Eng. Sci. 58 (2003) 2103.
[16] S.M. Yang, Y.E. Lee, S.H. Hyun, C.H. Lee, Organic-templating approach to synthesis of nanoporous silica composite membranes (I): TPA-templating and CO_2 separation, J. Mater. Sci. 37 (2002) 2519.
[17] Y.E. Lee, B.S. Kang, S.H. Hyun, C.H. Lee, Organic-templating approach to synthesis of nanoporous silica composite membranes (II): MTES-templating and CO_2 separation, Sep. Sci. Technol. 39 (15) (2004) 3541.